ELSEVIER

Journal of Alloys and Compounds 404–406 (2005) 89–94

Journal of ALLOYS AND COMPOUNDS

www.elsevier.com/locate/jallcom

Directional metal–hydrogen bonding in interstitial hydrides I. Structural study of $ErNi_3D_x$ ($0 \leq x \leq 3.75$)

Y.E. Filinchuk, K. Yvon*

Laboratoire de Cristallographie, Université de Genève, 24 quai E. Ansermet, CH-1211 Genève 4, Switzerland

Received 26 August 2004; received in revised form 3 December 2004; accepted 9 December 2004
Available online 19 July 2005

Abstract

Hydrogenation of $ErNi_3$ (space group $R\bar{3}m$) has been investigated by neutron powder diffraction on deuterided samples. At least three $ErNi_3D_x$ phases were found at deuterium compositions $x \sim 1.3$ (β_1), $x \sim 2$ (β_2) and $x \sim 3.8$ (γ), the latter being stable only under high deuterium pressure. Their structures show anisotropic lattice expansions and are non-centrosymmetric (space group $R3m$). In the β_1-phase, deuterium occupies two interstitial sites in the AB_2-type building block of which one provides three ligands of a Ni-centered NiD_4 tetrahedron and the other bridges a Ni triangle. In the β_2- and γ-phases, up to five new deuterium sites become partially occupied in both the AB_2- and AB_5-type building blocks. One of them provides the fourth ligand to the NiD_4 tetrahedron thus suggesting directional bonding effects similar to those observed in nickel-based complex metal hydrides, such as $LaMg_2NiH_7$ and Mg_2NiH_4.

Keywords: Hydrogen storage materials; Crystal structure and symmetry; Neutron diffraction

1. Introduction

Intermetallic compounds AB_3 (A = rare earth, Ca and Mg; B = Ni, Co and Fe) and their ternary derivatives usually crystallize with the hexagonal $CeNi_3$-type (space group $P6_3/mmc$) or the rhombohedral $PuNi_3$-type ($R3m$) structure. Both are built up by AB_5 (Haucke phase) and AB_2 (C14 Laves-Friauf phase)-type slabs. Upon hydrogenation they form various hydride phases (β, γ) that are called "interstitial" because hydrogen occupies various metal interstices in the AB_2 (β, γ) and AB_5-type (γ) slabs (for a recent review see Ref. [1]). Only few hydrides have been structurally characterized. The most complete study is that on the cobalt-based YCo_3-D system, which displays three rhombohedral hydride phases (β_1, β_2 and γ [2]). All have centrosymmetric structures ($R3m$). Among the nickel-based systems, structurally characterized compounds are rhombohedral $HoNi_3D_{1.8}$ [3] whose structure, however, is of unknown precision and hexagonal $CeNi_3D_{2.8}$ [4]. For the $ErNi_3$–H system, relatively detailed pressure-composition isotherms indicate at least two $ErNi_3H_x$ hydride phases. One (β) is stable under ambient conditions and displays a compositional range of $x = 2.2$–2.8 [5] (or $x = 1.9$–2.5 [6]) under ~1.3–15 bar hydrogen, while the other (γ) is unstable under ambient conditions and displays a compositional range of $x = 3.7$–5.5 at $-25\,^{\circ}C$ under 3–2000 bar hydrogen [7,8]. So far only cell parameters as determined from X-ray powder diffraction are available [6–8]. Here, we report on the synthesis and structure of three $ErNi_3H_x$ hydride phases (β_1, β_2 and γ) as studied by neutron powder diffraction on deuterides. It will be shown that they have non-centrosymmetric structures and display hydrogen configurations around the transition element that differ considerably from their cobalt analogues.

2. Experimental

2.1. Synthesis

Samples of nominal composition $ErNi_3$ were prepared by arc melting erbium (99.99%, Alfa) and nickel (>99.9%, Alfa) pieces under argon atmosphere, annealing the ingots

* Corresponding author. Tel.: +41 22 379 6231; fax: +41 22 379 6864.
E-mail address: klaus.yvon@cryst.unige.ch (K. Yvon).

0925-8388/$ – see front matter © 2005 Elsevier B.V. All rights reserved.
doi:10.1016/j.jallcom.2004.12.158

at 800 °C for 1 month (quartz tube, 1 bar argon) followed by quenching in cold water. X-ray powder diffraction showed that the samples were single-phase and consisted of the expected rhombohedral $ErNi_3$ phase. Deuteration (D_2 gas, 99.8%, AGA) was carried out in autoclaves at temperatures of −78, 20 and 80 °C and deuterium pressures of up to 100 bar for 2–7 days without preliminary activation. The reaction products were fine black powders and could be handled in air without detectable oxide formation. They consisted of three individual deuteride phases $ErNi_3D_x$ (referred to as β_1, β_2 and γ) as shown by X-ray analysis. No evidence for an appreciable solid solution of deuterium in the α-phase was found. In view of the relatively high equilibrium pressures (∼2–100 bar at room temperature) the samples desorbed deuterium so rapidly that their structure determination by conventional ex situ diffraction methods was not possible. Therefore, the samples were transported in autoclaves under deuterium pressure at a neutron source, or prepared on-site immediately before the diffraction experiments. Deuterium contents were estimated from X-ray measurements of rhombohedral cell volumes that varied in the ranges $V = 554$–559 Å^3 and 574–577 Å^3 for the β_1 and β_2-phases, and $V = 623$–635 Å^3 for the γ-phase. The coexistence of β_1 and β_2 phases in some samples confirmed that these were separate phases, such as those reported in the YCo_3-D system [2].

2.2. Structure characterization of deuterium-free $ErNi_3$

Diffraction data were collected for a 6 g sample on the neutron powder diffractometer HRPT at SINQ (PSI; Villigen) under standard conditions: cylindrical vanadium container, data collection time 8 h, high intensity mode, $\lambda = 1.15470(4)$ Å, 2θ range 4–164° ($d_{min} = 0.583$ Å), step size 0.05°. Structure refinement was carried out with the FULLPROF SUITE program package [9] based on the atomic coordinates of the $PuNi_3$-type structure (space group $R\bar{3}m$, two Er and three Ni sites). Attempts to refine the structure in non-centrosymmetric $R3m$ led to parameter oscillations around the centrosymmetric values, thus justifying the centrosymmetric choice. Refinement results are listed in Table 1.

2.3. Structure characterization of β_1-$ErNi_3D_{\sim 1.2}$

After the above experiment the alloy sample was refilled into a steel cylinder, connected to a deuteration system installed at PSI, evacuated for 1 h, deuterided at 10 bar and 150 °C for 5 h and gradually cooled to 20 °C during 20 h. The reacted powder was rapidly refilled into a V container, tightly sealed with indium wire and replaced on HRPT ($\lambda = 1.49418(3)$ Å, high intensity mode, 2θ range 4–164° ($d_{min} = 0.754$ Å), step size 0.1°, data collection time 10 h). Structure refinement confirmed the presence of ∼ 90% β_1-phase and ∼10% α-phase. Two deuterium atom positions were identified on nuclear difference density Fourier maps of the β_1-phase and their positions refined in space group $R\bar{3}m$. In spite of a relatively good fit ($R_B = 0.0340$, $R_F = 0.0258$, $\chi^2 = 5.55$, 35 parameters) the close proximity of two nearly half occupied deuterium sites (D–D ∼ 1.61 Å) in the structure suggested a loss of inversion symmetry. Refinements in non-centrosymmetric $R3m$ (three Er, five Ni and two D sites) lead to significantly lower R-factors ($R_B = 0.0224$, $R_F = 0.0157$, $\chi^2 = 3.59$, 40 parameters) and smaller standard uncertainties of the occupational and positional parameters of the deuterium sites. As expected, the latter sites were almost fully occupied and their closest distance was D1–D1 ∼ 2.45 Å. Atom coordinates and refinement results are listed in Table 2.

2.4. Structure characterization of β_2-$ErNi_3D_{\sim 2.0}$ and γ-$ErNi_3D_{\sim 3.8}$

After the above experiment, the sample was vacuum pumped at 80 °C for complete deuterium desorption, exposed to 100 bar of deuterium gas at 80 °C for about 1 day and then slowly cooled down to room temperature. It was kept under these conditions for 5 days and then transported in an autoclave under 100 bar deuterium pressure to PSI where it was rapidly refilled into a V container and tightly sealed with indium wire. Neutron diffraction data were collected on HRPT ($\lambda = 1.493814(19)$ Å, high intensity mode, 2θ range 4–157° ($d_{min} = 0.76$ Å), step size 0.1°, data collection time 11 h). Two phases, referred to as β_2- and γ, were identified in the pattern (Fig. 1). Up to seven deuterium sites were located on difference Fourier maps and their positions refined in centrosymmetric $R\bar{3}m$. Structure refinements in non-centrosymmetric $R3m$, such as with the β_1-phase were not feasible because of the small reflections-to-parameters ratio. On the other hand, the synthesis of a single-phase γ-deuteride sample was impracticable due to the very high deuterium equilibrium pressure (>20 bar) required for an

Table 1
Atomic coordinates and thermal parameters of $ErNi_3$[a] from neutron powder diffraction; e.s.d's in parentheses

Atom	Wyckoff site	x	y	z	$U_{eq/iso}$(Å^2)	U_{11} (Å^2)	U_{22} (Å^2)	U_{33} (Å^2)	U_{12} (Å^2)	U_{13} (Å^2)	U_{23} (Å^2)
Er1	3*a*	0	0	0	0.0081(9)	0.0079(8)	U_{11}	0.0085(11)	(1/2)U_{11}	0	0
Er2	6*c*	0	0	0.13923(7)	0.0085(6)	0.0071(5)	U_{11}	0.0113(8)	(1/2)U_{11}	0	0
Ni1	3*b*	0	0	1/2	0.0066(8)	0.0082(8)	U_{11}	0.0033(9)	(1/2)U_{11}	0	0
Ni2	6*c*	0	0	0.33309(7)	0.0077(6)	0.0086(6)	U_{11}	0.0059(7)	(1/2)U_{11}	0	0
Ni3	18*h*	0.5002(1)	$-x$	0.08222(4)	0.0069(2)	0.0063(2)	U_{11}	0.0080(3)	0.0034(2)	0.0003(2)	$-U_{13}$

[a] $R\bar{3}m$, $a = 4.94794(7)$, $c = 24.2909(5)$ Å, c/a ∼4.91, $V = 515.02(2)$ Å^3, all sites fully occupied, $R_B = 0.021$, $R_F = 0.015$, $\chi^2 = 1.99$, $R_p = 0.017$, $R_{wp} = 0.022$, 397 "independent" reflections, 119 "effective" (accounting resolution [9]) reflections; preferred orientation along [001] 1.036(3).

Table 2
Structure data for the non-centrosymmetric β_1-$ErNi_3D_{1.23}$[a] from neutron powder diffraction, e.s.d's in parentheses

Atom	Wyckoff site	x	y	z	$U_{eq/iso}$ (Å^2)	Occupancy
Er1	3*a*	0	0	−0.0008(4)	0.0068(6)	1.0(−)
Er21	3*a*	0	0	0.1311(4)	0.0051(5)	1.0(−)
Er22	3*a*	0	0	0.8692(4)	*U*(Er21)	1.0(−)
Ni1	3*a*	0	0	0.50000[b]	0.0055(6)	1.0(−)
Ni21	3*a*	0	0	0.3287(3)	0.0093(4)	1.0(−)
Ni22	3*a*	0	0	0.6621(3)	*U*(Ni21)	1.0(−)
Ni31	9*b*	0.4999(5)	−*x*	0.0726(2)	0.00505(18)	1.0(−)
Ni32	9*b*	0.5024(5)	−*x*	0.9190(3)	*U*(Ni31)	1.0(−)
D1	9*b*	0.5022(6)	−*x*	0.1368(3)	0.0172(9)	0.916(11)
D2	3*a*	0	0	0.2182(4)	*U*(D1)	0.952(18)

[a] Prepared at 20 °C and 10 bar deuterium pressure applied for a few hours, space group $R3m$, $a = 4.97180(7)$, $c = 25.9012(5)$ Å, $c/a \sim 5.24$, $V = 554.47(2)$ Å^3, $R_B = 0.022$, $R_F = 0.016$, $\chi^2 = 3.6$, $R_p = 0.015$, $R_{wp} = 0.019$; α-$ErNi_3D_x$ ($x < 0.1$): $V = 517.3(2)$ Å^3, $R_B = 0.035$; 410 "independent" reflections, 142 "effective" (accounting resolution [9]) reflections; refined phase contents: $\beta_1/\alpha = 0.88/0.12$.
[b] Fixed.

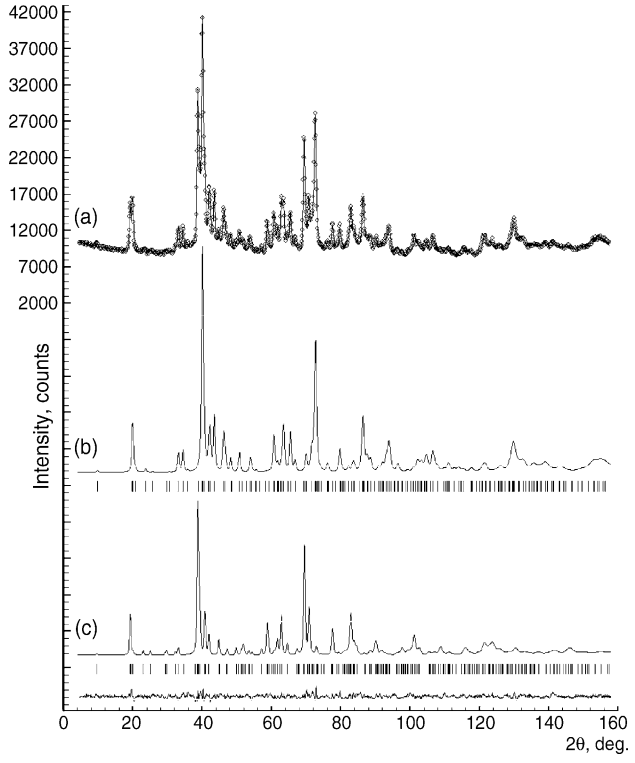

Fig. 1. Observed (points) and calculated (line) neutron diffraction patterns for an $ErNi_3$ sample deuterided at 100 bar (a), calculated patterns of the contributing phases β_2- (b) and γ-deuteride (c). Vertical bars indicate positions of Bragg peaks; difference pattern represented at the bottom; $\lambda = 1.493814(19)$ Å.

in situ study. Refinement results are listed in Table 3, and structural representations of the various phases are shown in Fig. 2.

3. Results and discussion

3.1. Composition and cell expansion

Similar to the cobalt system YCo_3-D [2] at least three deuteride phases (β_1, β_2, γ) occur in the $ErNi_3$-D system. Their ranges of existence as estimated from the present diffraction data are $x = 1.23$–1.33 (β_1), $x \sim 2$ (β_2) and $x = 3.44$–3.83 (γ), corresponding to a maximum hydrogen storage efficiency of ~ 1.1 wt.%. The upper limit of the relatively unstable γ-phase depends on deuterium pressure and can be estimated on geometrical grounds to be $x = 4.33$ (1.26 wt.% of hydrogen). The reported pressure-composition diagrams [5–7] support these findings, although they indicate somewhat higher hydrogen contents (by ∼0.5 H/f.u.) for all phases, including the solid solution α-phase for which the present data indicate $x < 0.1$. As for the cell parameters, those reported for $ErNi_3H_{1.9}$ [6] correspond to the present composition $ErNi_3H_{1.23}$, those reported for $ErNi_3H_{2.8}$ and $ErNi_3H_{1.1}$ [7] correspond to $ErNi_3H_{2.0}$ and hydrogen-free $ErNi_3$, respectively, and those reported for $ErNi_3H_{4.9}$ [8] to the lower limit of the γ-phase $ErNi_3H_{3.4}$. As with the cobalt system YCo_3D_x [2], the cell expansion is very anisotropic. While the increase of the axial ratio c/a at the α–β_1 transition can be attributed to the strong expansion of the AB_2 building block along *c*, its decreases at the β_1–β_2 and β_2–γ transitions can be attributed to the interplay between anisotropic expansions of the AB_2 and AB_5 building blocks. Strong expansion anisotropies are also observed in the nickel-based systems $HoNi_3D_x$ [3] and $CeNi_3D_x$ [4], while those in YNi_3D_x [10], $CaMg_2Ni_9D_x$ [11] and RFe_3H_x [12] are more isotropic.

3.2. Symmetry and interstitial D atom sites

Deuteration of $ErNi_3$ leads to a loss of inversion symmetry. This is the first time that such a symmetry loss is reported for a rhombohedral AB_3–H system. Although it has been experimentally ascertained only for the β_1-phase, it is likely to prevail also for the more deuterium-rich β_2- and γ-phases. Interestingly the β-$LaNi_5D_7$ phase, which constitutes the AB_5 slabs in the present structures, also lacks inversion symmetry (space group $P6_3mc$ [13]). This feature is presumably related to the propensity of nickel to adopt tetrahedral D environments (see Section 3.4). In contrast to the cobalt system YCo_3D_x that displays only three interstitial D sites, the nickel system $ErNi_3D_x$ displays up to seven. They

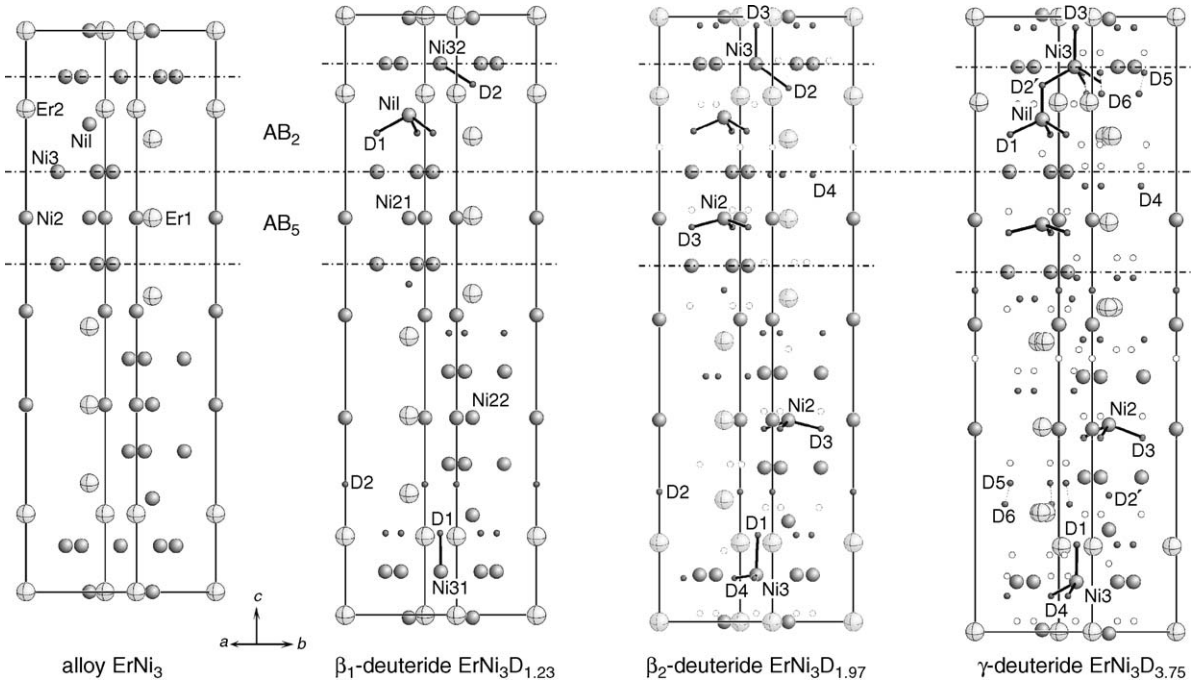

Fig. 2. Crystal structures of centrosymmetric $ErNi_3$ and non-centrosymmetric β_1-, β_2- and γ- $ErNi_3D_x$; β_2- and γ-structures refined in centrosymmetric space group $R\bar{3}m$; filled circles occupied D sites, open circles unoccupied D-sites in non-centrosymmetric model; Ni—D bonds shorter than ∼ 1.6 Å indicated by lines.

Table 3
Structure data for non-centrosymmetric β_2-$ErNi_3D_{1.97(4)}$ and γ-$ErNi_3D_{3.75(8)}$ as refined in centrosymmetric $R\bar{3}m$ from neutron powder diffraction, e.s.d's in parentheses

Atom	Wyckoff site	x	y	z	$U_{eq/iso}$ (Å^2)	Occupancy
β_2-$ErNi_3D_{1.97}$						
Er1	3*a*	0	0	0	0.0221(19)	1.0(−)
Er2	6*c*	0	0	0.1312(3)	0.0223(14)	1.0(−)
Ni1	3*b*	0	0	1/2	0.037(6)[a]	1.0(−)
Ni2	6*c*	0	0	0.3336(3)	0.0134(10)	1.0(−)
Ni3	18*h*	0.4992(5)	−*x*	0.07774(15)	0.0124(5)	1.0(−)
D1	18*h*	0.4910(12)	−*x*	0.1443(3)	0.020(2)	0.574(17)
D2	6*c*	0	0	0.2155(8)	*U*(D1)	0.385(19)
D3[b]	18*h*	0.50000	0.00000	0.0142(12)	*U*(D1)	0.135(8)
D4	18*h*	0.876(4)	−*x*	0.0725(14)	*U*(D1)	0.148(11)
γ-$ErNi_3D_{3.75}$						
Er1	3*a*	0	0	0	0.026(3)	1.0(−)
Er2[b]	18*h*	0.020(2)	−*x*	0.1391(4)	0.022	1/3(−)
Ni1	3*b*	0	0	1/2	0.0149(5)	1.0(−)
Ni2	6*c*	0	0	0.3299(3)	*U*(Ni1)	1.0(−)
Ni3	18*h*	0.4957(6)	−*x*	0.08159(17)	*U*(Ni1)	1.0(−)
D1	18*h*	0.493(3)	−*x*	0.1419(8)	0.038(−)	0.383(19)
D2	6*c*	0	0	0.2155	0.038(−)	0.06(3)
D2′	6*c*	0	0	0.4446(11)	0.038(−)	0.49(3)
D3[b]	18*h*	0.50000	0.00000	0.0173(6)	0.038(−)	0.361(18)
D4	18*h*	0.8405(16)	−*x*	0.0585(7)	0.038(−)	0.480(18)
D5	18*h*	*x*(D4)	−*x*	0.0911(13)	0.038(−)	0.303(19)
D6	18*h*	0.815(6)	−*x*	0.1255(19)	0.038(−)	0.185(17)

β_2 - $ErNi_3D_{1.97(4)}$: $a = 5.0456(3)$, $c = 26.157(3)$ Å, $c/a \sim 5.18$, $V = 576.70(8)$ Å^3, $R_B = 0.022$, $R_F = 0.015$; γ - $ErNi_3D_{3.75(8)}$: $a = 5.2398(3)$, $c = 26.605(2)$ Å, $c/a \sim 5.08$, $V = 632.60(8)$ Å^3, $R_B = 0.033$, $R_F = 0.024$; $\chi^2 = 4.3$, $R_p = 0.015$, $R_{wp} = 0.019$, 432 "independent" reflections, 115 "effective" (accounting resolution [9]) reflections; refined phase contents: β_2 / γ= 0.62/0.38.

[a] Ni1 atom was refined anisotropically in the β_2-deuteride: root-mean-square thermal displacement along *c* is two times higher than in a basal plane.
[b] Split atom positions: D3 split from 9*e* along *c* (D3-D3 ∼ 0.7–0.9 Å); Er2 split from 6*c* in basal plane (Er2–Er2 ∼ 0.32 Å).

Table 4
Interstitial deuterium sites, metal environments, occupancies, metal–deuterium distances, e.s.d's in parentheses

D sites[a] Metal environment	Occupancies metal–deuterium distances		
	β_1-$ErNi_3D_{1.23}$ ($R3m$)	β_2-$ErNi_3D_{1.97}$[b] ($R3m$)	γ-$ErNi_3D_{3.75}$[b] ($R3m$)
D1	92(1)%	*100%*	*77%*
$18h_7$ (AB_2 unit)	2Er21 2.490(3)	*2Er2 2.55*	*2Er2 2.63*
Trigonal bipyramid	Er22 2.216(9)	*Er2 2.15*	*Er2 2.18*
base: Er2Ni	Ni1 1.648(4)	*Ni1 1.50*	*Ni1 1.59*
apices: 2Er	Ni31 1.662(9)	*Ni3 1.74*	*Ni3 1.60*
D2	95(2)%	*77%*	
$6c_1$ (AB_2 unit) Tetrahedron	Er21 2.258(14)	*Er2 2.20*	
Er3Ni	3Ni32 1.703(7)	*3Ni3 1.80*	
D3		*27%*	*72%*
$18h_8$ (AB_5 unit)		*2Er1 2.55*	*2Er1 2.66*
Trigonal bipyramid		*Ni2 1.50*	*Ni2 1.56*
base: 3Ni		*Ni2 1.51*	*Ni2 1.61*
apices: 2Er		*Ni3 1.66*	*Ni3 1.71*
D4[c]		*30%*	*96%*
$18h_2$ (AB_2/AB_5)		*Er1 2.18*	*Er1 2.13*
Tetrahedron		*Er2 1.88*	*Er2 2.54*
2Er2Ni		*2Ni3 1.68*	*2Ni3 1.68*
D5[c]			*60%*
			Er1 2.82
			Er2 2.07
			2Ni3 1.59
D6			*37%*
$18h_3$ (AB_2 unit) Tetrahedron			*Er2 1.89*
2Er2Ni			*Er2 2.39*
			2Ni3 1.87
D2′			*98%*
$6c_3$ (AB_2 unit) Tetrahedron			*Ni1 1.47*
4Ni			*3Ni3 1.67*

[a] Notation according to Refs. [2,4] for centrosymmetric $R\bar{3}m$.
[b] Values in italics correspond to averages of centrosymmetric model; occupancies stated are those of the non-centrosymmetric model.
[c] D4 and D5 are ∼ 0.9 Å apart and occupy symmetry equivalent interstices in the centrosymmetric model, but are > 4 Å apart and occupy non-equivalent interstices in the non-centrosymmetric model.

show four-fold tetrahedral (D2: Er3Ni, D4-D6: 2Er2Ni, D2′: 4Ni) and five-fold trigonal bipyramidal (D1: 2Er3Ni, D3: 3Er2Ni) metal configurations (Table 4). In the β_1-phase, D1 (occupancy 0.92) and D2 (0.95) in the AB_2-type building block are almost fully occupied, while the AB_5-type block remains empty. In the β_2–phase, D1 becomes fully occupied (∼1.0 in the non-centrosymmetric model) while D2 starts to depopulate (∼0.8), and two new sites appear: D3 (∼0.3) in the AB_5 block and D4 (∼0.3) at the AB_2/AB_5 boundary. In the γ-phase D1 depopulates slightly (∼ 0.8) and D2 becomes almost empty (∼0.1) while D4 becomes fully occupied (∼1.0), D3 fills up (∼0.7) and three new sites are occupied at the AB_2/AB_5 boundary, D5 (∼0.6), and in the AB_2 block, D6 (∼0.4) and D2′ (∼1.0). The D5 and D6 sites occupy adjacent interstices (D5–D6 ∼ 0.9 Å) and thus cannot be occupied simultaneously. Interestingly, the cobalt systems YCo_3D_x [2] and $ErCo_3D_x$ [14] show distinctly different deuterium occupancies. Both structures are centrosymmetric. In β_1-$YCo_3D_{1.24}$ and β_2-$YCo_3D_{2.0}$, only one site (D1) in the AB_2 block is occupied while in γ-$YCo_3D_{4.6}$ and $ErCo_3D_{4.1}$ two additional sites, D4 at the AB_2/AB_5 boundary and D3 in the AB_5 block, are occupied. The remaining three sites occupied in the nickel compound (D2, D6 and D2′) are not occupied in the cobalt compound. This leads to significantly different D atom configurations around the transition elements (see Section 3.4).

3.3. Interatomic distances

The loss of inversion symmetry in the β_1-phase leads to a significant distortion of the metal matrix as shown by the Ni–Ni bonds that are no longer equivalent (Ni1–Ni31 ∼ 2.83, Ni1–Ni32 = 2.63 Å). Similar differences presumably also occur in the β_2- and γ-phases although they have not been ascertained experimentally due to a lack of resolution. As expected the Ni–Ni bonds bridged by D ligands expand considerably, such as Ni1–Ni31 ∼ 2.83, while those not bridged are less affected, such as Ni2–Ni3 = 2.46 and Ni3–Ni3 = 2.45–2.49 Å. The shortest metal–deuterium distances involving nearly fully occupied D-sites are Ni–D = 1.59 and Er-D = 2.18 Å. The shortest D–D contacts are 1.88 Å (D4–D4).

3.4. Transition metal environment and directional Ni–D bonding

Among the five Ni sites, all have D ligands except Ni21 and Ni22 in the β_1-phase (see Fig. 2). The most striking configuration is that around Ni1 which consists of three D1 ligands in the β_1-and β_2-phases and is completed by a forth ligand (D2′) to a Ni-centered NiD_4 tetrahedron in the γ-phase. A similar but more disordered tetrahedral configuration also occurs around Ni32 (D2′, D3, 2D5 and 2D6) in the γ-phase. Three-fold configurations reminiscent of the incomplete tetrahedral configuration around Ni1 in the β_1-and β_2-phases occur around Ni21 and Ni22 in the β_2- and γ-phases (3D3) and around Ni31 in the β_2- and γ-phases (D1 and 2D4). A two-fold configuration occurs around Ni32 (D2 and D3) in the β_2 phase, and single D ligands occur with Ni31 (D1) and Ni32 (D2) in the β_1 phase. The only Ni atoms without D ligands are Ni21 and Ni22 in the β_1 phase. The D–Ni–D bond angles in the NiD_4 tetrahedrons are in the range 100–115° and suggest directional bonding effects similar to those in complex hydrides, such as Mg_2NiH_4 and $LaMg_2NiH_7$ [15]. As expected, these effects are similar to those in the nickel-based analogue β-$HoNi_3D_x$ [16] but differ from those in the cobalt analogues β_1-, β_2- and γ-YCo_3H_x [2] in which the transition metal shows octahedral hydrogen coordination. Note that the deuterium contents and atomic radii in the cobalt and nickel systems are similar and thus can hardly account for these structural differences. This demonstrates that hydrogen atom distributions in so-called “interstitial” metal hydrides cannot be rationalized by geometrical considerations alone but need to take into account preferred transition metal–hydrogen configurations.

Acknowledgements

This work was supported by the Swiss National Science Foundation and the Swiss Federal Office of Energy. The authors thank Professor K. Ross for communicating a preprint of his work. This work was partly performed at the Swiss Spallation Neutron Source SINQ, Paul Scherrer Institute, Villigen, Switzerland. The authors thank Dr. D. Sheptyakov (PSI, Villigen) for help with neutron diffraction measurements.

References

[1] M. Latroche, A. Percheron-Guégan, J. Alloys. Compd. 356–357 (2003) 461.
[2] J. Liu, P.A. Georgiev, D.K. Ross, M. Roberts, K.A. Andersen, M. Telling, D. Fort, Phys. Rev. B, submitted for publication.
[3] V.V. Burnasheva, V.A. Yartys’, S.P. Solov’ev, N.V. Fadeeva, K.N. Semenenko, Sov. Phys. Crystallogr. 27 (1982) 409.
[4] V.A. Yartys, O. Isnard, A.B. Riabov, L.G. Akselrud, J. Alloys Compd. 356–357 (2003) 109.
[5] A. Goudy, W.E. Wallace, R.S. Craig, T. Takeshita, Adv. Chem. Ser. 167 (1978) 312.
[6] V.V. Burnasheva, B.P. Tarasov, Russ. J. Inorg. Chem. 1982 (27)1077.
[7] V.N. Verbetsky, S.N. Klyamkin, A.Y. Kovriga, A.P. Bespalov, Int. J. Hydrogen Energy 21 (1996) 997.
[8] S.A. Lushnikov, S.N. Klyamkin, V.N. Verbetsky, J. Alloys Compd. 330–332 (2002) 574.
[9] J. Rodriguez-Carvajal, FULLPROF SUITE, LLB Sacley & LCSIM Rennes, France, 2003.
[10] K.H.J. Buschow, R.H. van Essen, Solid State Commun. 32 (1979) 1241.
[11] K. Kadir, N. Kuriyama, T. Sakai, I. Uehara, L. Eriksson, J. Alloys Compd. 284 (1999) 145.
[12] C.A. Bechman, A. Goudy, T. Takeshita, W.E. Wallace, R.S. Craig, Inorg. Chem. 15 (1976) 2184.
[13] C. Lartigue, A. Le Bail, A. Percheron-Guegan, J. Less-Common Met. 129 (1987) 65.
[14] V.V. Burnasheva, V.V. Klimeshin, K.N. Semenenko, Inorg. Mater., Transl. from Izv. Akad. Nauk. SSSR, Neorg. Mater. 15 (1979) 197; V.V. Burnasheva, V.V. Klimeshin, V.A. Yartys’, K.N. Semenenko, Inorg. Mater., Transl. from Izv. Akad. Nauk. SSSR, Neorg. Mater. 15 (1979) 627.
[15] G. Renaudin, L. Guénée, K. Yvon, J. Alloys Comp. 350 (2003) 145.
[16] Y. Filinchuk, D. Sheptyakov, K. Yvon, J. Alloys Compd., 2005, in press.